MOONS – multi-object spectroscopy for the VLT: Spectrograph Performance

M. Black, R. Artan, C. Breen, K. Campbell, L. Chapman, et al.

Published version information:

Citation: M Black et al. MOONS – multi object spectroscopy for the VLT: spectrograph performance. Proc SPIE 12184 (2022): 121847A. Is in proceedings of: Ground-based and Airborne Instrumentation for Astronomy IX, Montréal, Québec, Canada, 17-22 Jul 2022

DOI: 10.1117/12.2629802

MOONS – multi-object spectroscopy for the VLT: spectrograph performance

M. Black, R. Artan, C. Breen, K. Campbell, L. Chapman, et al.

M. Black, R. Artan, C. Breen, K. Campbell, L. Chapman, S. Chittick, M. Cliffe, G. Davidson, O. Gonzalez, R. Kotlewski, C. Lawrence, D. Lee, J. Moffat, N. O'Malley, P. Rees, R. Sharman, J. Strachan, G. Tait, W. Taylor, C. Waring, R. Waterston, G. Wilks, "MOONS – multi-object spectroscopy for the VLT: spectrograph performance," Proc. SPIE 12184, Ground-based and Airborne Instrumentation for Astronomy IX, 121847A (29 August 2022); doi: 10.1117/12.2629802

SPIE.

Event: SPIE Astronomical Telescopes + Instrumentation, 2022, Montréal, Québec, Canada

MOONS – multi-object spectroscopy for the VLT: Spectrograph Performance

M. Black[a*], R. Artan[a], C. Breen[a], K. Campbell[a], L. Chapman[a], S. Chittick[a], M. Cliffe[a], G. Davidson[a], O. Gonzalez[a], R. Kotlewski[a], C. Lawrence[a], D. Lee[a], J. Moffat[a], N. O'Malley[a], P. Rees[a], R. Sharman[a], J. Strachan[a], G. Tait[a], W. Taylor[a], C. Waring[a], R. Waterstone[a], G. Wilks[a]

[a]STFC UK ATC, Royal Observatory Edinburgh, Blackford Hill, Edinburgh, EH9 3HJ, UK

ABSTRACT

MOONS is a Multi-Object Optical and Near-infrared Spectrograph currently under construction as a third generation instrument for the Very Large Telescope (VLT). It combines the large collecting area offered by the VLT (8.2m diameter), with a large multiplex and wavelength coverage (optical to near-IR: 0.8μm - 1.8μm). Integration of 2 of the arms of the spectrograph (RI and YJ) was recently completed at the UK Astronomy Technology Centre, and initial engineering tests carried out to assess the performance of the spectrograph. This paper presents an overview of the system, the integration and alignment process, and an assessment of the image quality of the two cameras, wavelength coverage and resolving power.

Keywords: Spectrograph, Ground-based instruments, multi-object infrared spectrographs, integration process.

1. INTRODUCTION

The Multiple-Object Optical and Near-infrared Spectrograph (MOONS) is a new instrument being constructed for installation at the Nasmyth focus of the European Southern Observatory's Very Large Telescope (VLT). MOONS is designed to be a powerful spectroscopic survey instrument and has several key design features to maximize survey efficiency: it will observe the full 25 arc-minute field of view of the VLT, it will simultaneously observe up to 1,000 objects, and it will capture spectra over the broad wavelength range 650 nm to 1,800 nm.

The instrument consists of three sub-systems: the rotating front end, the spectrograph, and the control software. A full description is provided in [1] and [2]. The rotating front end is so called because it will be mounted to the Nasmyth rotator on the VLT. It contains a large field corrector lens, the focal plate with 1,000 fibre positioning units, field acquisition cameras, a metrology system, electronics, cable wrap and the calibration system [3]. There is a fibre link between the rotating front end and the spectrograph [4][5]. The spectrograph consists of two three-channel spectrographs mounted either side of an optical bench. Each three-channel spectrograph contains a slit, collimator, dichroic beam splitters, dispersing optics, and three cameras covering RI, YJ and H-bands [6]. The RI-band cameras are fitted with 4096 by 4096 pixel CCDs from LBNL, and the YJ and H-band cameras are fitted with 4096 by 4096 pixel MerCadTel detectors, Teledyne H4RG [7]. The entire spectrograph is housed within a large cryogenic vacuum chamber that cools the optical bench to an operational temperature of 130 K and the H4RG detectors to 40 K. MOONS has a sophisticated electronics control system [8] and the control software includes complex algorithms to perform simultaneous movements of all 1,000 fibre positioners [9].

This paper will describe the spectrograph design, including an overview of the vacuum and cryogenic system, the integration and alignment process of the subsystems on the optical bench, and the performance assessment of the RI and YJ cameras that have been fitted thus far.

* martin.black@stfc.ac.uk

Ground-based and Airborne Instrumentation for Astronomy IX, edited by Christopher J. Evans, Julia J. Bryant, Kentaro Motohara, Proc. of SPIE Vol. 12184, 121847A
 · 0277-786X · doi: 10.1117/12.2629802

2. INSTRUMENT DESIGN OVERVIEW

Figure 1 shows a recent photo of the first side of the optical bench that has been populated. Since the photograph was taken the gratings and prisms have been fitted to the H disperser mechanism.

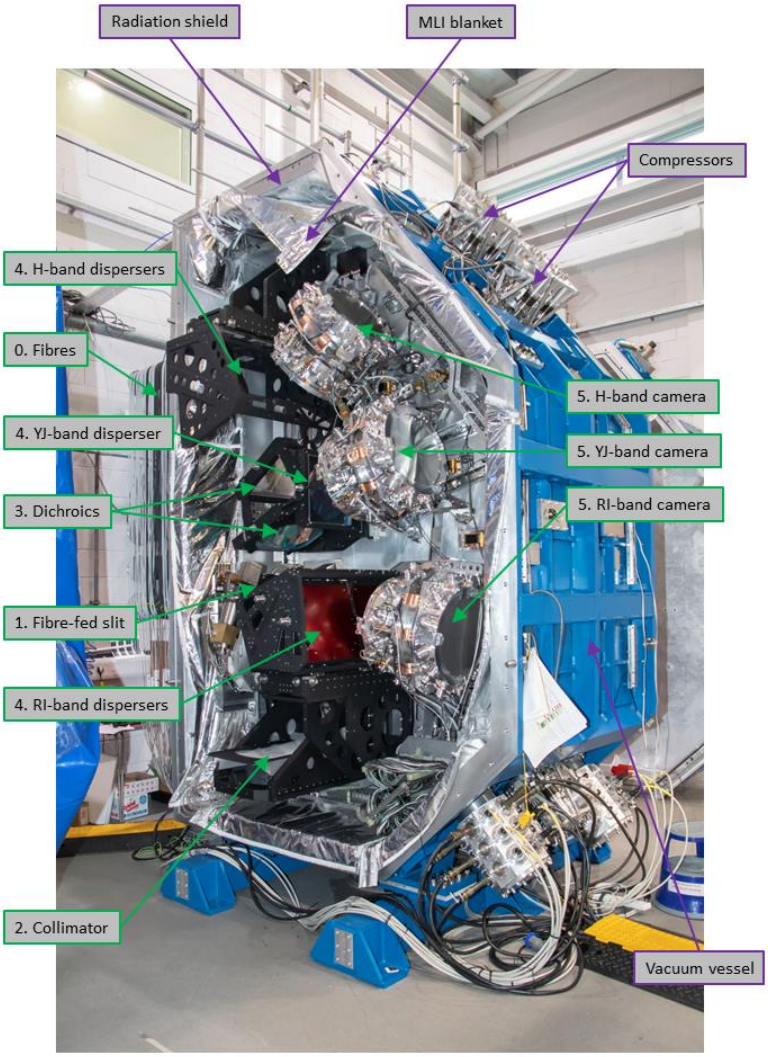

Figure 1: Overview of MOONS cryostat showing internal components on one side of system.

The optical fibre bundles are currently stored on a series of drums mounted on a temporary structure attached to the front of the cryostat. This ensures the 32 bundles, which vary in length from 18 to 24 metres, are kept safe from damage, while allowing access to all the ends of the fibres to be illuminated for testing. Eventually these fibre bundles will be connected to the positioning units in the rotating front end via a cable chain. The bundles then enter the cryostat via individual vacuum feedthroughs mounted on a common interface flange before then forming the slit of the spectrograph, shown in Figure 2.

The collimator mirror is mounted below the slit and reflects the collimated beam back up over the slit, to the “fixed optics” module consisting of two dichroic filters, to separate the three wavelength channels, and the dispersing element for the YJ channel. Above and below this module are mounted two “grating exchange systems” that contain both high- and low-resolution dispersing optics for the H and RI wavelength channels respectively. The three cameras are also mounted on the optical bench, in line with these systems. This is all duplicated on the opposite side of the optical bench. A detailed description of the optical design of the overall system, and the cameras, can be found in [1].

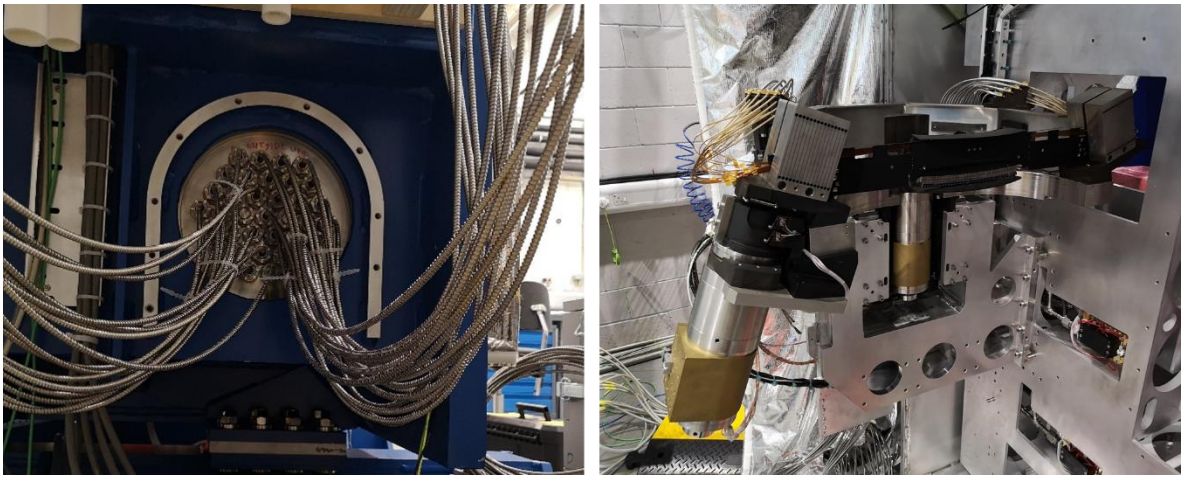

Figure 2: Left, vacuum fibre feedthroughs on common flange. Right, slit assembly inside cryostat.

In addition to the optical subsystems all the electrical services and various cold fingers are mounted on the optical bench to provide power, control, and appropriate cooling.

3. CRYOGENIC AND VACUUM SYSTEM OVERVIEW

The MOONS vacuum chamber is around 2.3 m long, 2.2 m width, and 3.5 m high, with an internal volume of around 18 m^3. It is a welded construction made from 5083 aluminum. The vessel consists of a central section with mounting feet to the Nasmyth platform, within which the optical bench is mounted. This is then completed by two clamshell doors, that attach either side of the central section, to form the enclosure. A similarly constructed radiation shield, wrapped in a segmented MLI blanket, sits between the outer vessel and optical bench. The vacuum pump set consists of two ATH 2303M Turbo pumps each backed by an ACP 40 roots pump, one set mounted on each door, as shown in Figure 3. The pressure achieved in 24 hours after evacuation begins is in the mid 10^{-5} mbar. Base pressure when warm is in the 10^{-6} mbar range, which then drops into the 10^{-7} mbar range when cold.

The MOONS cold mass is made up of, approximately, 500 kg of 6082 aluminum radiation shield, 1800 kg of 6082 aluminum optical bench and 1400 kg of glass optics and mounts. This is cooled to an average temperature of 135 K in 48 hours using a liquid nitrogen precool system. The system consists of a high level 'bath' manifold with the exhaust fed directly to atmosphere. The bath manifold feeds 8 pairs of pads on the optical bench and 2 pairs of pads on the radiation shield. The pads are filled simultaneously by the bath manifold and are spaced over the optical bench to give a uniform cooling across the bench. At the telescope the system will be fed via liquid nitrogen dewars, and an automated switchover system will be used, to allow cooling to take place overnight with minimal intervention.

Once the system reaches a set of defined temperatures, the precool switches itself off and the temperature is held cold using 3 Cryomech 10MD cryocoolers. Two of these are directly attached to the radiation shield and the third to the optical bench. The bench is set to run at 134 K in deference to the CCD detectors which are not permitted to drop below 130 K. The radiation shield is allowed to cool in an uncontrolled manner and settles out at 76-120 K. The single cryocooler is responsible for cooling a large mass and so there is a relatively large time constant required for changes to the bench temperature. It is worth noting that the infrared detectors are cooled to their operating temperature, 40 K, using a controlled ramp once the pre-cooling is complete. This ensure they are not exposed to dangerous thermal shocks.

Although the bench itself has a low thermal gradient, the temperature of some of the assemblies mounted to the bench lags behind the bench. Consequently, it takes a further 7-10 days for the temperatures to stabilise to less than 1 K/day change at the cameras. While this temperature gradient influences the system performance, the rate and effect of this change diminishes over the 7-10 days, meaning the system reaches working condition prior to this complete stabilisation.

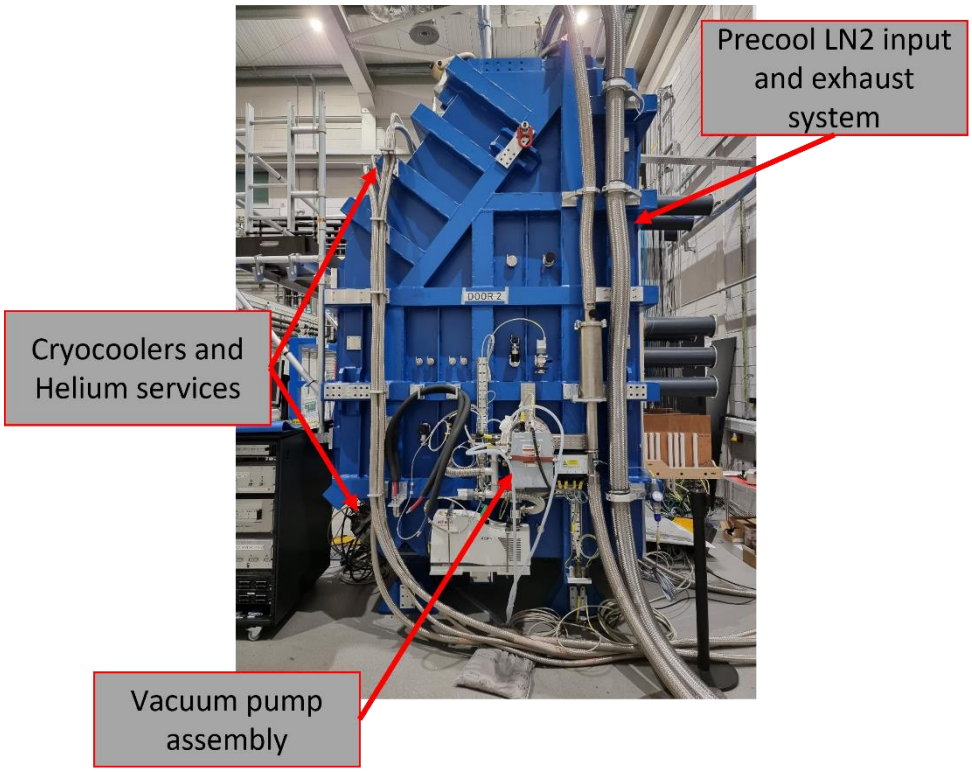

Figure 3: Side view of vessel with vacuum, precool, and cooling system identified.

4. INTEGRATION AND SUBSYTEM ALIGNMENT

The detailed alignment of the fibre system the alignment of the cameras is covered in other papers in this conference. These were delivered to the UK Astronomy Technology Centre with test reports confirming compliance with the system specifications, and as such no further adjustment to those systems was made. The alignment strategy of the remaining parts, and for the sub-systems relative to one another on the optical bench relied on physical measurements, and adjustments, as opposed to any active optical alignment.

The fundamental principle was to measure the optics locations relative to common reference points on the bench, and position these such that it matched the nominal as built optical model. Given the complexity of mounting these parts there are several stages to achieve this. First the optical mounting "hard points" are measured and related to the references on each optic mounting bracket or frame. These could then be adjusted such that the optical component was located correctly within the mount, to an appropriate tolerance (which vary between components from 500µm to around 50µm on the pads to control angles). In the case of the fixed optics assembly the three optics within their frames were then mounted on a common plate. These were then aligned to one another using references on the frames and base plate. This is shown for the fixed optics in Figure 4, and similar systems were employed on all outstanding parts. Measurements were carried out using a FARO portable CMM arm, or a Leica AT403 laser tracker, with various SMR balls and nests.

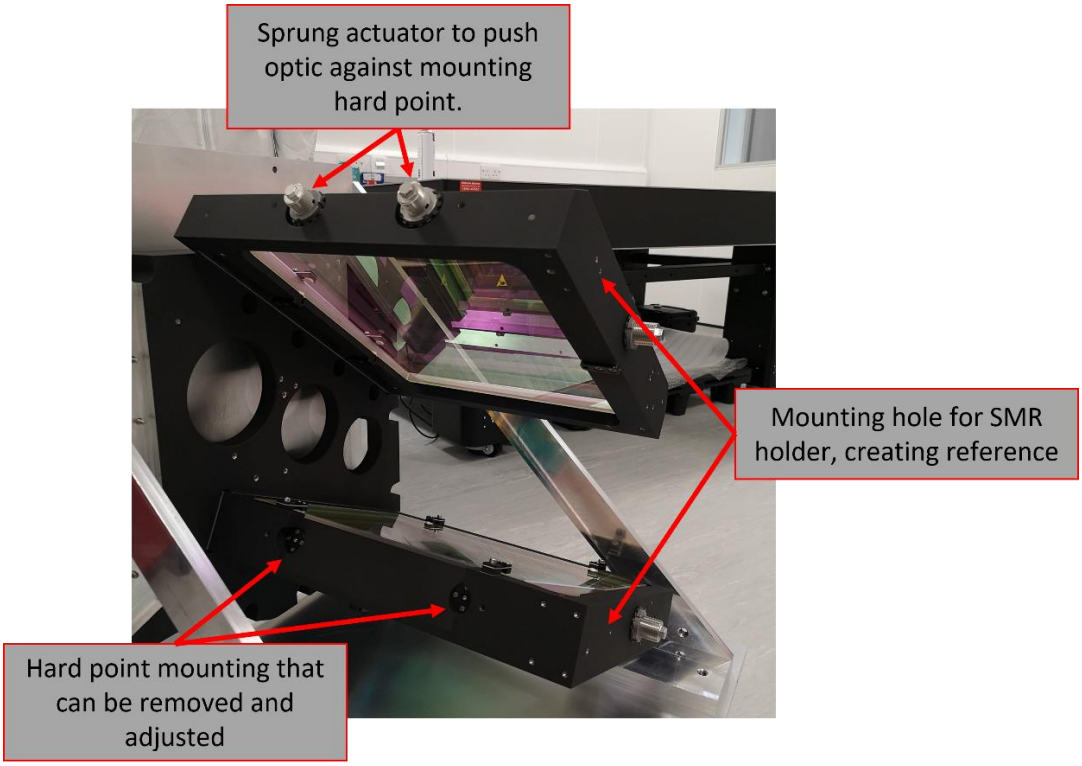

Figure 4: Fixed optics assembly with dichroic filters fitted, showing optics mounting points and reference marks.

With each optical sub-system self consistently aligned where required, the process to position them all on the optical bench could take place. It is worth considering the difficulties that are introduced in doing this due to the size and weight of the components. The collimator mass is 138 kg, each camera has a mass of 120 kg, the fixed optics are 121 kg, and the slit assembly 70 kg, which is also complicated by having all the fibre bundles attached during integration. All of these required a crane lift to locate onto the bench, and in many cases additional special tools or cantilever lifting arms to access the mounting locations. Figure 5 shows the fixed optics and a camera being lifted into position using some of these tools. Note that the lifting point on the fixed optics is located on the base plate in the centre of all the optics. This requires additional care when fitting or removing but provides the most secure lift. Figure 5 also shows one of the disperser assemblies during a test lift to establish the best method of installation, before any optics were integrated. This proved to be an essential step to ensure confidence in handling once the optics were installed. Aluminum dummy masses were placed in the mounts to ensure the center of gravity and mass was correct during test lifts.

In all cases the sub-systems are mounted against 3 pins located on the optical bench, with steel blocks forming the interface between the part and the pin. These blocks are removable and can be machined to provide accurate lateral offsets of the sub-system. Rotation and distance from the bench are also controlled via sacrificial machinable shims. The parts were fitted with nominal shims in place, and then the location was measured using the same references as before and related to reference points on the optical bench using the laser tracker and targets. This data can then be analysed and compared to the system opto-mechanical model, identifying offsets required to nominally locate all parts. This process could be repeated to ensure the mounting was repeatable and consistent between fittings. It was shown to be possible to locate all parts to the required tolerances within one or two adjustments. While the option of micrometer push adjusters was considered, the size and weight of the parts would have made such an approach very difficult and risky. Relying on machinable hard shims formed the baseline approach instead.

Figure 5: UK ATC technicians fitting the fixed optics assembly (top left), RI disperser (top right), and camera (lower).

5. PERFORMANCE AGAINST REQUIREMENTS

At present both the RI and YJ cameras, and all required parts for these two channels, on the first side of the optical bench have been fitted and characterised. There are various requirements which the system must meet to achieve its science goals, however the key ones to consider in this context are the image quality, essentially defining the spectral sampling, the spectral resolving power, and the wavelength coverage. Another consideration is the requirement for a clear definition between adjacent fibres, avoiding cross contamination. Testing for these two channels was carried out using a tungsten halogen lamp to provide a broadband source, and an Argon emission lamp to provide spectral lines across the wavelength range. These lamps were set up near the output fibres and could be used to illuminate the system in two ways. It is possible to illuminate all fibres simultaneously by removing the protective caps on each bundle and illuminating the area of the floor to which the fibres are pointing. While this does not provide equal illumination levels to all bundles the dynamic range of the detector system is sufficient for this to not to be an issue. The other method uses a set of extension fibres to selectively illuminate specific fibres across the slit. Normally 5 fibres are illuminated in this way, sampling along the spatial direction of the slit.

Testing began by using the 5 individual fibres, illuminated by the Argon lamp, to create a grid of points (regions of interest) across the image that can be used to determine image quality and measure focus. The detectors are attached to the camera module using three motorised actuators around the perimeter of the camera. These motors are progressively stepped over a range of focus positions, recording an image at each plane. Given the cameras are faster than F/1 the depth of focus is very sensitive. As such, a first focus position within the full 2 mm range of travel is estimated by eye. Once within this range the actuator positions are scanned in 10 µm steps over a limited range. The Full Width Half Maximum (FWHM) of the arc line images at each actuator position are then computed and plotted. The FWHM minima for each arc line image across the field can then be found. It would be expected that due to mounting tolerances a tip/tilt adjustment of the detector plane would be necessary to optimise focus. This tip/tilt is calculated, and an offset applied to account for the actuators being located around 250 mm from the centre of the detector. This analysis has been automated, and the outputs are shown in Figure 6. This output allows the actuators positions to be set, and the focus quality verified. It is worth noting that the variance between each actuator position needed to induce this tilt is on the scale of 50 µm across the actuators.

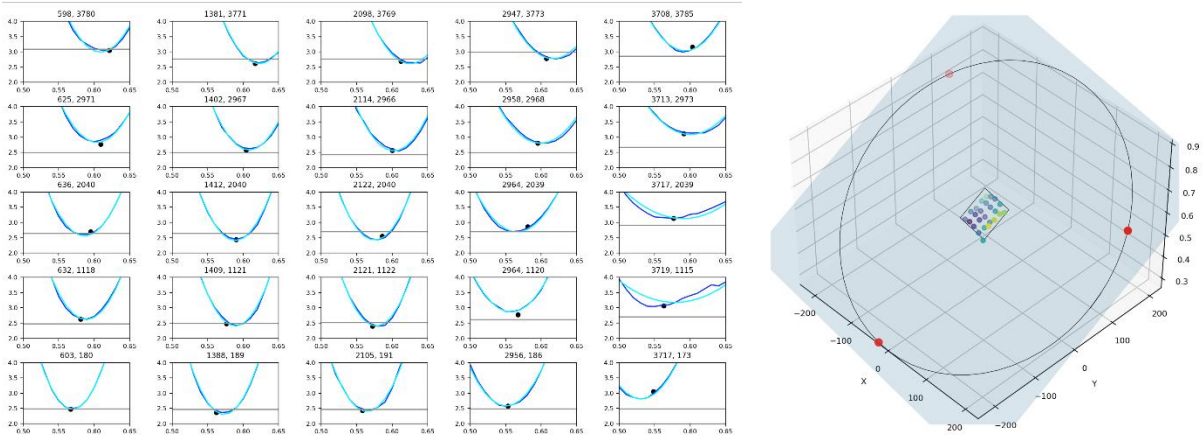

Figure 6: Left - plots of image FWHM (ordinate) through different detector actuator positions (abscissa) for YJ camera, and right - calculated best fit detector tip/tilt image plane.

It was mentioned previously that due to the size of the system there is a time lag between the bench reaching operating temperature, and the other components reaching steady state. Even once the temperature sensors on the outside of the mechanism report a steady state it was thought that the glass optical components might still be cooling. To monitor this the system was set to good focus at the end of one phase of cold testing. This camera was then left untouched during the subsequent warm phase. Then on the next cool down the image recorded on the camera was compared to the last image taken on the previous cool down. Figure 7 shows the change in image FWHM over several days after the detector is at its operating temperature. The rate of change diminishes to a level that should not affect testing after a few days, which sets a baseline wait time after cooling before starting for all future test and observation campaigns. Once in operation at the telescope the system will remain cold unless an intervention of the spectrograph system is required.

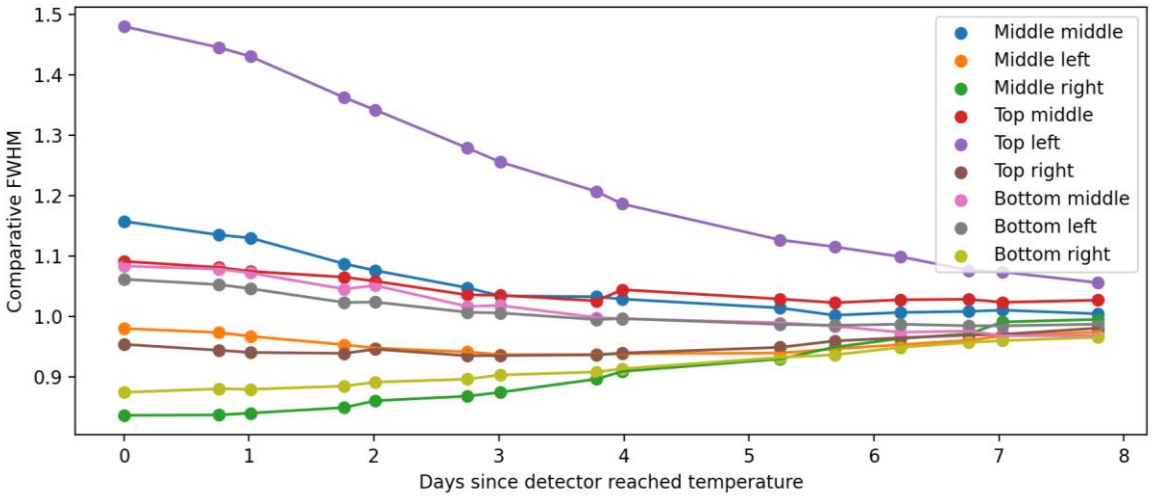

Figure 7: Plot showing change in image FHWM against time due to thermal settling of the instrument.

Once the system had been shown to have settled and no longer changing due to thermal effects, performance analysis could take place. To verify all fibres were transmitting light the system was fully illuminated using the tungsten halogen lamp. A image containing the spectra of all 512 fibres is shown in Figure 8.

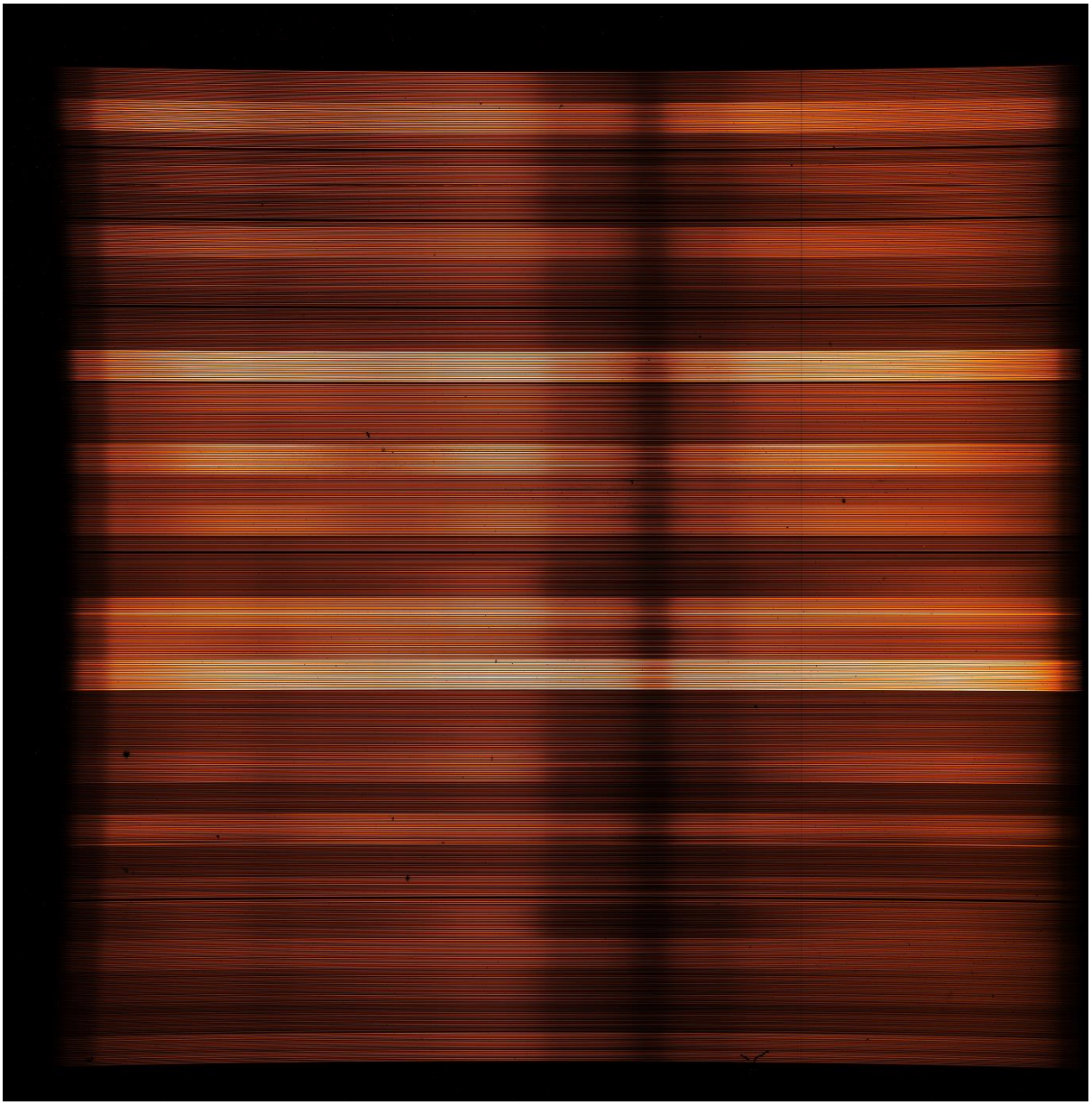

Figure 8: Broadband spectrum seen in the YJ camera when all fibres in the slit are illuminated. Note; image banding is likely caused by output screen/print resolution. The dark area in the centre of the spectra is caused by plastic protective end caps that were left on the bundle ends during this test.

Various positive results could be derived from the image in Figure 8. Firstly, all fibres, except those already known to be damaged in production, could be seen. The alignment of the spectral dispersion to the detector rows was within a few pixels, and the entire slit is well centred in the field of view. Clear dark areas can also be seen between each spectra, indicating low cross contamination between adjacent fibres, Figure 9.

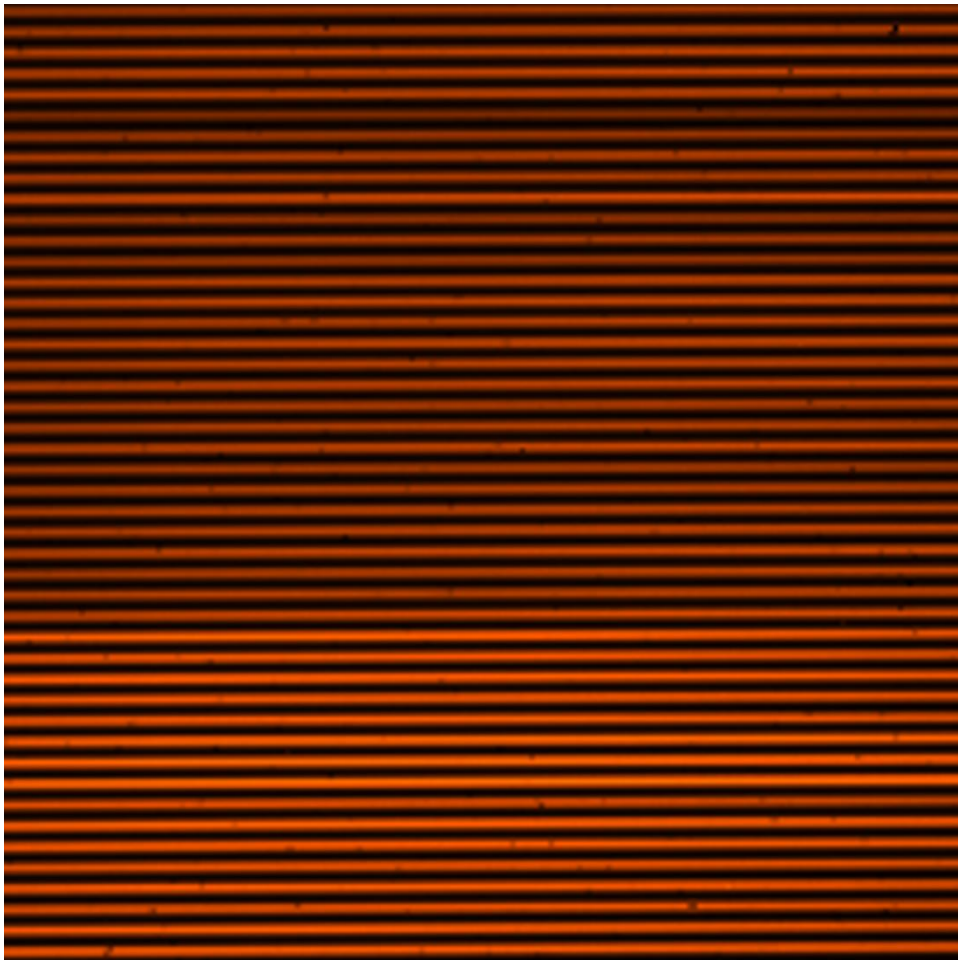

Figure 9: Zoom in on subset of broadband illuminated fibres showing dark regions between individual spectra.

In terms of more quantifiable results, using the Argon lamp the image quality produced by the system can be assessed. Figure 10 shows plots of images of isolated lines in three fibres taken across the full field of the instrument in the YJ channel, and an overlay between the end-to-end simulation of a region of the spectrum to real data. The resultant images vary between 2.5 pixels FWHM in the centre and 2.7 pixels FWHM at the corners of the detector. In the RI channel the images are 2.5 pixels FWHM in the centre, reaching 3 pixels FWHM in the corners. Both results are in line with expected performance in the optical design, as can be seen in the match between the simulated and real data. This confirms that requirements for image quality and spectral sampling are fulfilled by the spectrograph optical system.

Again, using the Argon lamp, the wavelength range coverage and resolving power, Figure 11, could be assessed. In both cases, across the YJ and low-resolution RI channels, both the wavelength coverage and spectral resolving power requirements (the latter being R~4000) have been met.

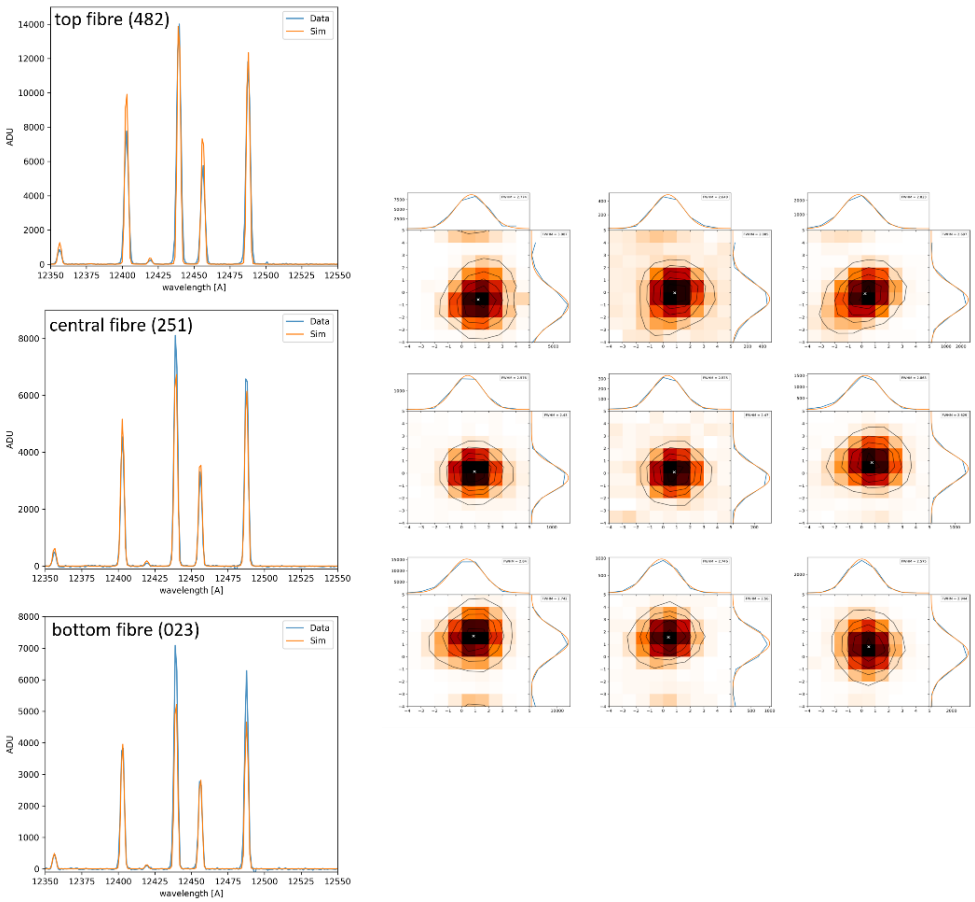

Figure 10: A 3x3 grid of images created by isolated spectral in the YJ channel showing good image quality, and three plots over laying end to end simulation data with real data, the match indicating as predicted spectral sampling.

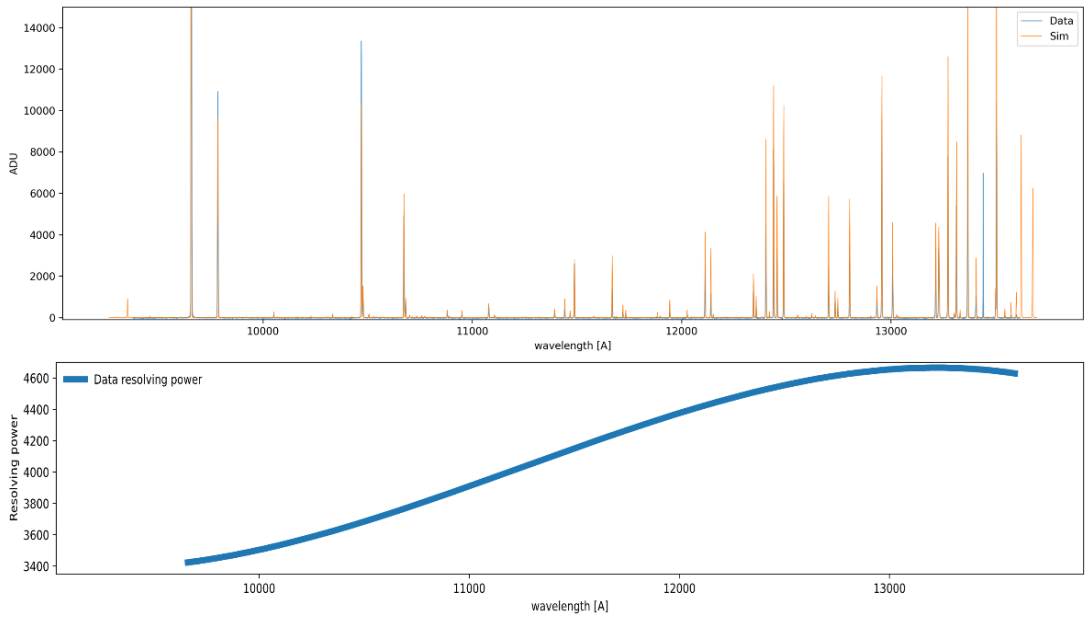

Figure 11: Plot of resolving power against wavelength over the range of the YJ channel. The expected value at the centre of the range is 4000.

6. SUMMARY AND CONCLUSIONS

This paper has summarized the current build status, alignment methods, and performance of the MOONS spectrograph. The two channels on the first side that have been tested have met all the requirements set upon them, and this has been achieved without additional alignment between cooldowns. This is a testament to both the quality of the manufacturing and alignment of the sub-systems upon delivery, and confirmation of the validity of the alignment strategy being employed.

Currently the third camera, the first H band system, is being fitted for testing. Once this has been tested it will allow the assessment of the first half of the system to take place and sign off one set of all the optical components. Assuming the performance is comparable to the previous two channels it gives good confidence that the second side should perform similarly. The assessment of these will take place on the next major cooldown once all outstanding parts have been received and integrated. Additional testing on the mechanisms is planned, as well as an assessment of the higher resolution dispersing elements (relating to wavelength coverage and resolving power) using a Thorium-Argon lamp to provide greater line density in these regions.

REFERENCES

[1] M. Cirasuolo, et al., "Crescent MOONS: an update on the ongoing construction of the new VLT's multi-object spectrograph," Proc. SPIE 11447, Ground-based and Airborne Instrumentation for Astronomy VIII, 1144717 (13 December 2020); https://doi.org/10.1117/12.2561229

[2] W. Taylor et al., "Rising MOONS: an update on the VLT's next multi-object spectrograph as it begins to grow," Proc. SPIE 10702, Ground-based and Airborne Instrumentation for Astronomy VII, 107021G (13 July 2018); https://doi.org/10.1117/12.2313403

[3] A. Cabral et al., "MOONS, the next ESO VLT's multi-object spectrograph: the field corrector and the rotating front end," Proc. SPIE 11447, Ground-based and Airborne Instrumentation for Astronomy VIII, 114478D (13 December 2020); https://doi.org/10.1117/12.2561412

[4] I. Guinouard, D. Horville, D. Lee, S. Watson, P. Rees, and H. Flores, "Assemblies of the microlenses on the front-end fibres of MOONS," Proc. SPIE 11451, Advances in Optical and Mechanical Technologies for Telescopes and Instrumentation IV, 114516I (13 December 2020); https://doi.org/10.1117/12.2560639
[5] I. Guinouard, J-P. Amans, D. Horville, D. Lee, A. Cabral, P. Rees, S. Watson, W. Taylor, and H. Flores, "Final characteristics and performances of the fibres of MOONS," Proc. SPIE 11451, Advances in Optical and Mechanical Technologies for Telescopes and Instrumentation IV, 114516J (13 December 2020); https://doi.org/10.1117/12.2560635
[6] E. Oliva, B. Delabre, A. Tozzi, D. Ferruzzi, D. Lee, I. Parry, and P. Rees, "Toward the final optical design MOONS, the Multi-Object Optical and Near infrared Spectrometer for the VLT," Proc. SPIE 9908, Ground-based and Airborne Instrumentation for Astronomy VI, 99087R (9 August 2016); https://doi.org/10.1117/12.2231388
[7] D. Ives, D. Alvarez, N. Bezawada, E. George, B. Serra, "Characterisation, performance and operational aspects of the H4RG-15 near infrared detectors for the MOONS instrument," Proc. SPIE 11454, X-Ray, Optical, and Infrared Detectors for Astronomy IX, 114541N (13 December 2020); https://doi.org/10.1117/12.2562408
[8] P. Gutierrez, D. Atkinson, S. Beard, and N. Di Lieto, "Ethernet to multi-CAN gateway for VLT MOONS instrument control," Proc. SPIE 11452, Software and Cyberinfrastructure for Astronomy VI, 114522A (13 December 2020); https://doi.org/10.1117/12.2557215
[9] L. Makarem, J-P. Kneib, and D. Gillet, "Collision-free coordination of fiber positioners in multi-object spectrographs," Proc. SPIE 9913, Software and Cyberinfrastructure for Astronomy IV, 99130V (26 July 2016); https://doi.org/10.1117/12.2231716